# A Robust Demand Regulation Strategy for DERs in a Single-Controllable Active Distribution Network

Shah Fahad, Arman Goudarzi, Rui Bo, *Senior Member, IEEE*, Muhammad Waseem, Rashid Al-Ammari, and Atif Iqbal, *Fellow, IEEE*

***Abstract*—Over the past decade, PQ regulation schemes for a single-controllable active distribution network (ADN) using coordination among a network of virtual synchronous generators (VSGs) have been proposed. However, considering the variable nature of intermittent renewable energy sources (IRESs), coupling a cluster of IRESs with the point of common coupling (PCC) of ADN could inflict transient issues for the power management of the whole ADN. To counter these challenges, the proposed study has three main objectives: 1) To propose a modified mathematical model that represents the apparent resistance-reactance at the PCC of ADN in relation to the PQ coordination among the network of VSGs; 2) to utilize the proposed model for deriving a $\mu$ synthesis-based robust controller that overcomes the uncertainty in the moment of inertia response of all the VSGs; 3) and to present the stability and performance analysis of the proposed controller validated under model uncertainty. Validation of the proposed method and its comparison to the state-of-the-art methods in MATLAB/Simulink environment confirms that the proposed method significantly minimizes the impact of disturbances on the power management of the whole ADN.**

***Index Terms*—$\mu$-synthesis, hierarchical control, networked virtual synchronous generator (VSG) control, robust control, single-controllable active distribution networks (ADNs).**

## I. Introduction

In THEpast decade, the power systems have witnessed a tremendous rise in integration of intermittent renewable energy sources (IRESs) into the power systems. As per the global status report 2021 in [1], a total of 243 GW of photovoltaic generators and 77 GW of wind turbine generators (WTGs)-based new power plants were installed around the globe in the year 2022. Integrating IRESs on such a large scale can enable distributed power management systems throughout the power systems in the upcoming years. As a consequence, distributed power management systems could overcome problems with conventional power systems that are fully centralized in nature. Moreover, the distributed energy resources (DERs) can subdue the need of long transmission lines thus mitigating huge losses. However, replacing the conventional synchronous generators (SGs) with converter-interfaced DERs can introduce power quality challenges for the power systems. These challenges include voltage rise issues due to reverse power flow, no/low inertial response, and unconsumed power from maximum power point tracking (MPPT) enabled DERs. Solving these challenges may require a more innovative approach towards designing new control strategies that could tackle the aforementioned challenges. For this purpose, the proposed study presents a new approach to overcome the influence of generation from the IRESs on the point of common coupling (PCC) of active distribution networks (ADNs).

The aforementioned challenges can greatly be overcome by introducing coordination among DERs. For this purpose, it is pertinent to operate the DERs without MPPT module. In this manner, DERs will produce power according to the desired demand reference from the distribution system operator (DSO) [2]. Coordination among non-MPPT operated DERs can unlock various power management and optimization features for ADNs [3].

A rising concern in the modern power systems is the lack of inertial response due to IRESs. The progressive rise in the penetration levels of IRESs is replacing the SGs-based generation. The IRESs lacks the massive rotating rotor which is the key inertia element of conventional power systems. By replacing the SGs with converter-interfaced IRESs, the inertia constant of the overall power systems is declining. With the high penetration of IRESs, the power systems will experience the frequency nadir in shorter time period as compared to SGs oriented power systems. Also, lower inertia constant increases the rate of change of frequency (RoCoF) which could lead to frequent tripping of protection relays even for minor disturbances [4]. The moment of inertia of a SG is constant due to its physical nature, while in VSG-based system the virtual inertia parameter is tuned to a fixed value. However, the virtual inertia performance is dependent upon the available energy. In case enough energy is not available to overcome the impact of a disturbance, the virtual synchronous generator (VSG) will not be able to supply the intended virtual inertia according to the control design. Therefore, even if the virtual inertia term is tuned to a fixed value, the IRES may not supply the intended virtual inertia due to its intermittent nature.

Furthermore, recent studies have proposed to control the PCC of ADNs through constant active and reactive power (PQ)

Manuscript received 20 July 2023; revised 5 December 2023; accepted 14 March 2024. Date of publication 10 April 2024; date of current version 20 June 2024. This work was supported by the NPRP under Grant 13S-0108-200028 from the Qatar National Research Fund (a member of Qatar Foundation). *(Corresponding author: Shah Fahad.)*

Shah Fahad and Rui Bo are with the Missouri University of Science and Technology, Rolla, MO 65409 USA (e-mail: shah.fahad@mst.edu; rbo@mst.edu).

Arman Goudarzi and Muhammad Waseem are with the University of victoria, Victoria V8P 5C2, Canada, and also with the Maynooth University, W23 F2H6 Maynooth, Ireland (e-mail: arman.goudarzi@gmail.com; muhammad.waseem@mu.ie).

Rashid Al-Ammari and Atif Iqbal are with the Qatar University, Doha 2713, Qatar (e-mail: ralammari@qu.edu.qa; atif.iqbal@qu.edu.qa).

Digital Object Identifier 10.1109/JSYST.2024.3379856

injection/consumption to/from the grid, respectively. The demand at PCC is fulfilled by the PQ generation from DERs. The PQ regulation at PCC of ADNs mimics the behavior of constant power load (CPL) [5]. It is commonly known that the CPLs experience the negative incremental impedance effect (NIIE) which exhibits a nonlinear relation between voltage and current. This nonlinearity will risk the stability of the PCC parameters when major disturbances occur such as high variation in PCC demand or load, and, fluctuation in output power from DERs.

Moreover, the PQ demand at PCC is normally dispatched to the DERs through unidirectional broadcast communication. This method couples the PCC to the DERs. The PCC of ADN, if coupled with the IRESs, the NIIE can be intensified. The generation or load variations in the system will introduce spikes in the PQ regulation at PCC of ADN. Moreover, the synthetic moment of inertia of IRESs will also influence the PQ regulation at PCC because the amount of time the DERs take to respond to the changes in the system will influence the PQ demand at PCC. For this purpose, it is pertinent that the controller used for PCC regulation should be robust against uncertainties in moment of inertia of IRESs.

The aforementioned problems are prominent reasons of reduction of rigidness of parameters at PCC of ADN. For a distributed power management system, satisfactory performance of voltage and current parameters at each PCC will aid to the overall performance of the power systems. Taking this scenario as a base, the regulation of PCC parameters satisfied by coordinated PQ generation from non-MPPT operated DERs within an ADN can unlock various optimization and energy management opportunities for distributed power management systems.

### *A. Literature Review*

The base of the proposed study is to enhance the rigidness of parameters at the PCC of ADN. However, the proposed study considers the simultaneous satisfaction of two objectives. One is achieving satisfactory performance of the PQ coordination among DERs while simultaneously regulating the PCC demand. It is necessary to emphasize on the difference between the proposed hierarchical control architecture and the conventional voltage and frequency ($V/f$) restoration-based hierarchical control methods for microgrids [6]. The proposed method involves grid connected system where only regulation of apparent resistance and reactance (RX) at PCC of ADN is focused while $V/f$ restoration methods are mainly applied to islanded microgrids [7], [8]. Therefore, comparing the proposed method with the conventional hierarchical control methods for frequency/voltage restoration stands irrelevant.

From the perspective of parameters regulation at PCC, several coordination control strategies have been presented in the literature. For instance, in [9], an energy management system (EMS) is presented for a distributed power management scheme of a microgrid comprising of PV, battery energy storage system (BESS), and a proton-exchange membrane fuel cell. This strategy successfully implements coordination among converter-interfaced sources; however, the simultaneous regulation of parameters at PCC of microgrid is ignored. The authors in [10], [11], [12], and [13] have proposed different EMS techniques to utilize the BESS for suppressing the influence of intermittent power from IRESs. These techniques successfully inject constant power to the grid; however, they lack coordination among DERs. It is pertinent to recall here that, the proposed method considers the simultaneous implementation of coordination among DERs and the parameters regulation at PCC of ADN. In [14], the authors presented a power quality enhancement approach through EMS technique. However, this method strictly relies on a converter directly interfaced to the PCC of the ADN.

In [14], a power management strategy that enhances the power quality of the overall system was presented. Nevertheless, to successfully implement this strategy, a converter is required to be directly connected to the PCC.

The authors in [15] and [16] attempted to implement coordination among IRESs using distributed control techniques. These distributed control strategies only considered active power management while it is commonly known that the voltage regulation can be deteriorated if reactive power management is ignored.

Some of the studies in [17], [18], and [19] proposed coordination control strategies by using parallel operating VSGs. Although, these strategies focused on coordination among VSGs; however, the regulation of the PCC of ADN was not considered. On the contrary, the authors in [20] presented the PCC regulation strategy; nonetheless, coordination among VSGs is not considered.

A few studies proposed simultaneous implementation of PCC regulation and coordination among DERs. For instance, the authors in [21] presented a coordination control scheme for a cluster of grid feeding converters and simultaneously regulating the PCC of ADN as a constant PQ node. Clearly, the use of grid feeding converters deteriorate the inertial response of the power systems. Moreover, the reactive power from DERs is utilized to achieve voltage balancing. However, voltage balancing is achieved at the cost of disproportionate reactive power sharing among DERs which ultimately leads to poor power factor for distant DERs from the substation. To subdue the aforementioned shortcomings, the authors in [3], [5], and [22] proposed proportionate sharing of active and reactive powers from grid forming converters to regulate the PCC of ADN as a constant PQ node. However, the authors in [23] reported a major challenge of NIIE on the PCC parameters due to PQ regulation of ADN. To counter the NIIE, the authors in [23] proposed a control strategy to regulate the PCC of ADN as a constant apparent RX node using coordination of parallel operating grid forming converters. Although, this method performed satisfactorily in terms of overcoming the NIIE; however, the parameters at PCC of ADN still experiences serious oscillations during disturbances such as power variation from IRESs, load variation, and/or demand variation at PCC of ADN. In addition, this method did not considered the element of uncertainty in the moment of the inertia of IRESs. Oscillations in parameters confirm the lack of rigidness at PCC of ADN. If the oscillations are not suppressed, they can reduce the life expectancy of the substation transformer as well as the DERs due to their limited power ratings based converters.

For the concerns mentioned above, the proposed study aims to enhance the rigidness of the parameters at PCC of ADN using $\mu$ synthesis-based control technique. For this purpose, this study presents an extension to the strategy proposed in [22] and [23]. First, this study modifies the mathematical model presented in [22], and utilizes the modified model to build a concatenated plant model. The modified model considers the dynamics of the parallel operating converters (all DERs) on the demand management error at PCC of ADN. Second, a $\mu$ synthesis-based robust controller is derived that minimizes the $H_\infty$ norm of the closed-loop system considering the uncertainties in moment of inertia of DERs. Third, it has been shown that, the proposed concatenated plant is internally stable, and robust against the uncertainty in moment of inertia from each DER, and it enhances the rigidness of the PCC even against severe disturbances. Finally, to confirm the superiority of the proposed model, a comparison with the state of the art methods is presented. The major contributions of the proposed study are enlisted as follows.

1) To extend the idea proposed in [22], this study modifies the mathematical model of PQ regulation at PCC for the application of apparent RX demand regulation at PCC of ADN. Superior to PQ regulation strategy, this extended mathematical representation allows robust apparent RX demand regulation at PCC, consequently, enhancing the rigidness of overall parameters at PCC of ADN.
2) Using the extended model, this study then derives a $\mu$ synthesis-based controller which is robust against the uncertainties in moment of inertia from DERs and it successfully minimizes the $H_\infty$-norm of the closed-loop concatenated plant model.
3) Finally, the stability and performance analysis of the extended plant model in closed-loop with the derived controller is presented. Furthermore, a detailed comparative analysis of the proposed method with state-of-the-art methods [5], [22], [23] is presented to confirm the superiority of the proposed robust controller.

The rest of this article is organized as follows. Section II reviews the basic preliminaries of the hierarchical control structure proposed for this method. The mathematical modeling for the proposed method is given in Section III. Results and discussion is given in Section IV. Finally, Section V concludes this article.

## II. Preliminaries of the Hierarchical Control Structure

This study proposes a modification in the secondary control of the hierarchical control strategy presented in [22] and [23]. However, the role of the primary and secondary control layer in the hierarchical control architecture cannot be disregarded. Moreover, the influence of the dynamics of the ADN on the PCC regulation also needs detailed analysis. Therefore, for the sake of clarity, the primary and tertiary control structures, along with the influence of the dynamics of the ADN on the PCC regulation are introduced in the subsections below.

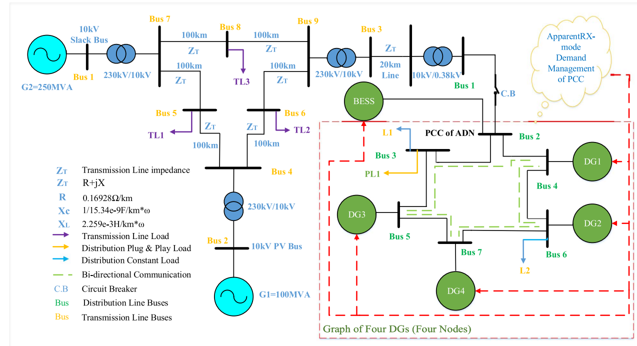


Fig. 1. Test system to validate the proposed hierarchical control strategy.

### A. Primary Control Layer

The proposed hierarchical control strategy is validated on the test system given in Fig. 1. It can be observed from this figure that, the ADN is being energized by several VSG controlled DERs that operat without MPPT device. The VSG control uses the swing equation to mimic the behavior of a SG. The electromechanical equation and the excitation control used by the VSG in the proposed study can be expressed as

$$J_{\text{vsg}}\omega_{\text{vsg}}\frac{d\omega_{\text{vsg}}}{dt} = P_{\text{ref}} - P_e - D(\omega_{\text{vsg}} - \omega_g) \tag{1}$$

$$K_{\text{inertia}}\frac{dE^d_{\text{ref}}}{dt} = (Q_{\text{ref}} - Q_{\text{vsg}}) + K_q(|V_g| - V^d_{\text{vsg}}). \tag{2}$$

Here, $J_{\text{vsg}}$, $\omega_{\text{vsg}}$, $\omega_g$, and, $K_{\text{inertia}}$ is the moment of virtual inertia, virtual mechanical shaft's angular frequency, grid's angular frequency, and the excitation controller's virtual inertia constant, respectively; $P_{\text{ref}}$), $P_{\text{vsg}}$, and $E^d_{\text{ref}}$ represents the virtual mechanical power, electrical power of the VSG, and reference voltage of the converter-interface, respectively; the terms $D$, $K_q$, and, $Q_{\text{vsg}}$ denotes the virtual damping, reactive power droop constant, and reactive power of VSG, respectively.

The term $J_{\text{vsg}} = \frac{2H_{\text{vsg}}S_{\text{vsg}}}{\omega^2_{\text{vsg}}}$ in (1) is dependent upon the apparent power ($S_{\text{vsg}}$) of the VSG which is not fixed due to the intermittent nature of the IRESs. Therefore, this study considers the impact of uncertainty in the virtual moment of inertia on the PCC of ADN. Differentiated by the control strategy used for the DERs, the overall inertia including the virtual inertia from DERs can be expressed by

$$H_{\text{sys}} = \sum_{i=1}^{n_s} H_{\text{SG}i} * \frac{S_{Gi}}{S_{\text{sys}}} + \sum_{i=1}^{n_d} H_{\text{DER}i} * \frac{S_{\text{DER}i}}{S_{\text{sys}}} + \sum_{i=1}^{n_d} H_{\text{BESS}i} * \frac{S_{\text{BESS}i}}{S_{\text{sys}}}. \tag{3}$$

Here, the subscript $''i''$ represents the $i$th term; $S_{Gi}$, $S_{\text{DER}i}$, $S_{\text{BESS}i}$ denotes the apparent power of SG, DER, and BESS, respectively; the inertia constant of SG, DER, and the BESS is represented by $H_{\text{SG}i}$, $H_{\text{DER}i}$, $H_{\text{BESS}i}$, respectively. Although, the virtual inertia constant of the individual VSG can retain the overall power system's inertia, however, the proposed study utilizes coordination of a cluster of VSGs. In this manner, the virtual inertia from VSG controlled DERs is provided by the whole cluster rather than an individual DER. In the proposed study, the primary control layer (1)–(2) of each DER receives active and reactive power reference from the secondary and tertiary control layers as

$$P_{\text{ref}} = P_{i\text{sec}-\text{ref}} + P_{i\text{Ter}-\text{ref}}; Q_{\text{ref}} = Q_{i\text{sec}-\text{ref}} + Q_{iTer-\text{ref}}. \quad (4)$$

Here, the terms $P_{i\text{sec}-\text{ref}}$, and $P_{i\text{Ter}-\text{ref}}$ denotes the active power references dispatched from the secondary and tertiary control layers, respectively; the terms $Q_{i\text{sec}-\text{ref}}$ and $Q_{i\text{Ter}-\text{ref}}$ represents the reactive power references dispatched from the secondary and tertiary control layer.

### B. Tertiary Control Layer

As already discussed in the previous section, the proposed method uses a cluster of non-MPPT operated DERs. However, DERs without MPPT requires proper instructions for active and reactive power dispatch. For this purpose, the proposed study uses consensus-based distributed control algorithm where each DER will exchange information with the neighboring DER. The bidirectional information exchange is achieved through graph theory. Using the consensus-based distributed control algorithm, a proportionate active and reactive power sharing among DERs can be achieved. The distributed controller will vary the active and reactive power references at each iteration using the equation given by [24]

$$P_{i\text{Ter}-\text{ref}}(k+1) = P_i(k) + \rho \sum_{j=1}^{n} -l_{i,j}\alpha_j(k), \quad (5a)$$

$$Q_{i\text{Ter}-\text{ref}}(k+1) = Q_i(k) + \sigma \sum_{j=1}^{n} -l_{i,j}\beta_j(k) \quad (5b)$$

where $P_i(k)$ is the active power and $Q_i(k)$ is the reactive power of $i$th DER, respectively, during current iteration; $P_{i\text{Ter}-\text{ref}}(k+1)$ is the active power and $Q_{i\text{Ter}-\text{ref}}(k+1)$ is the reactive power of $i$th DER, respectively, during the next iteration.

Consensus indexes for the active and reactive powers is given by $\alpha = \frac{P}{P^*}$ and $\beta = \frac{Q}{Q^*}$, respectively. Here, $P^*$ and $Q^*$ denotes the available active and reactive power while the $P$ and $Q$ represents the output active and reactive power from respective DER. A consensus is considered to be reached, if the index of all the DERs converge a common value.

### C. System Dynamics and PCC Regulation

The main priority of the proposed strategy is to regulate the PCC of ADN as a constant apparent RX node with an enhanced rigidness property. The apparent impedance demand at PCC of ADN can only be fulfilled if the following expression is satisfied:

$$\frac{v_{\text{pcc}}}{Z^*_{\text{ref}}} = \sum_{j\epsilon S_E}^{n} i_{Gj} - \sum_{i\epsilon S_L}^{n} i_{Li} - i_{\text{loss}} = i_m. \quad (6)$$

Here, the voltage at PCC is given by $v_{\text{pcc}}$; the apparent impedance demand reference at the PCC is given by $Z^*_{\text{ref}}$.

Eq. (6) can be used to extract *dq* components of the voltage and current. For instance, the term $v_{d-\text{pcc}}$ can be extracted from $v_{\text{pcc}}$. Similarly, from $Z^*_{\text{ref}}$, $R^*_{\text{ref}}$ can be taken to extract the *d*-axis reference current at PCC. In this manner, the term $v_{d-\text{pcc}}/R^*_{\text{ref}} = i^*_{d-\text{pcc}}$. In addition, $X^*_{\text{ref}}$ from $Z^*_{\text{ref}}$ can be used to calculate the *q*-axis reference current such that $v_{d-\text{pcc}}/X^*_{\text{ref}} = i^*_{q-\text{pcc}}$. The terms $R^*_{\text{ref}}$ and $X^*_{\text{ref}}$ are the demand references for the apparent resistance and reactance at PCC of ADN. In (6), the current generation from the $j$th DER, $i$th load current consumption, and losses (from $i^2R$) are represented by $i_{Gj}$, $i_{Li}$, and $i_{\text{loss}}$, respectively. In the same equation, $i_{\text{pcc}}$ is the current injection/consumption (depending on the sign convention) at PCC in *dq*-axis frame. If $v_{d-\text{pcc}}/R^*_{\text{ref}} = i_{d-\text{pcc}}$ and $v_{d-\text{pcc}}/X^*_{\text{ref}} = i_{q-\text{pcc}}$, this condition shows that the apparent RX demand at PCC is satisfied. In other words, the apparent RX demand at PCC will be fulfilled by the cluster of DERs and BESS, if $i^*_{d-\text{pcc}} = i_{d-\text{pcc}}$ and $i^*_{q-\text{pcc}} = i_{q-\text{pcc}}$.

From (6) it can be observed that, there are three dynamic elements that will influence the apparent RX demand satisfaction. The system disturbances, such as power variation from IRESs (which also influences its moment of inertia response, load demand consumption variation, and apparent RX demand variation required by the DSO/TSO, will introduce an error in the apparent RX demand regulation at PCC such that $i^*_{d-\text{pcc}} \neq i_{d-\text{pcc}}$ and $i^*_{q-\text{pcc}} \neq i_{q-\text{pcc}}$ until the new error in the demand is reduced to zero. In response to the disturbances, the amplitude of error introduced in the apparent RX regulation and the time taken the error to reduce to zero shows the rigidness of the PCC. To conclude, if the PCC experiences larger oscillations, then the PCC is termed as less rigid and vice versa [22].

## III. Proposed Robust Control Approach

### A. Apparent RX Regulation At PCC

In the proposed strategy, apparent RX regulation at PCC of ADN is considered. The prime concern of the proposed robust control strategy is to enhance the rigidness of the apparent RX regulation at PCC. As per *dq*-frame parameters, the instantaneous active and reactive power at PCC can be expressed as

$$P_{\text{pcc}} = 1.5 v_{d-\text{pcc}} i_{d-\text{pcc}}; Q_{\text{pcc}} = -1.5 v_{d-\text{pcc}} i_{q-\text{pcc}}. \quad (7)$$

Here, $v_{d-\text{pcc}}$, $i_{d-\text{pcc}}$, and $i_{q-\text{pcc}}$ denote the *d*-axis voltage at PCC, *d*-axis current at PCC, and *q*-axis current at PCC, respectively. According to ohm's law, $i_{d-\text{pcc}}$ and $i_{q-\text{pcc}}$ can be written as

$$i^*_{d-\text{pcc}} = v_{d-\text{pcc}}/R^*_{\text{ref}}; i^*_{q-\text{pcc}} = v_{d-\text{pcc}}/X^*_{\text{ref}}. \quad (8)$$

Here, $i^*_{d-\text{pcc}}$ and $i^*_{q-\text{pcc}}$ are the *dq*-frame reference currents calculated using the apparent resistance ($R^*_{\text{ref}}$) and reactance ($X^*_{\text{ref}}$) demand values. As discussed in the previous section, the steady-state condition shows that $i^*_{d-\text{pcc}} = i_{d-\text{pcc}}$ and $i^*_{q-\text{pcc}} = i_{q-\text{pcc}}$. Considering the steady-state condition and using (8), $i_{d-\text{pcc}}$ and $i_{q-\text{pcc}}$ in (7) can be replaced and rearranged as

$$R = 1.5 v^2_{d-\text{pcc}}/P_{\text{pcc}} \quad (9a)$$

$$X = -1.5 v^2_{d-\text{pcc}}/Q_{\text{pcc}}. \quad (9b)$$

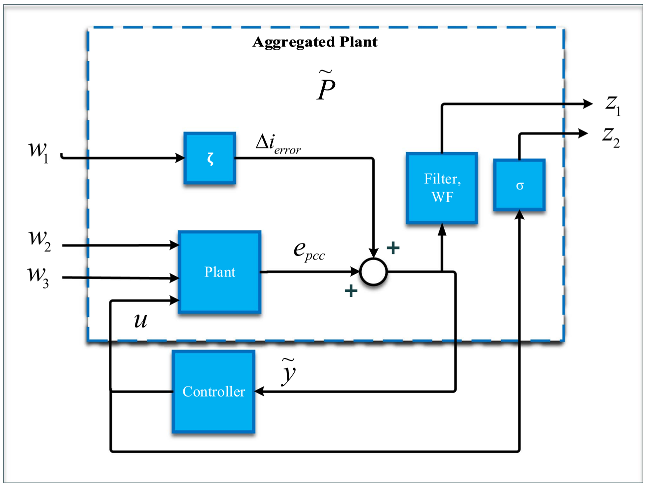


Fig. 2. $\mu$ control problem.

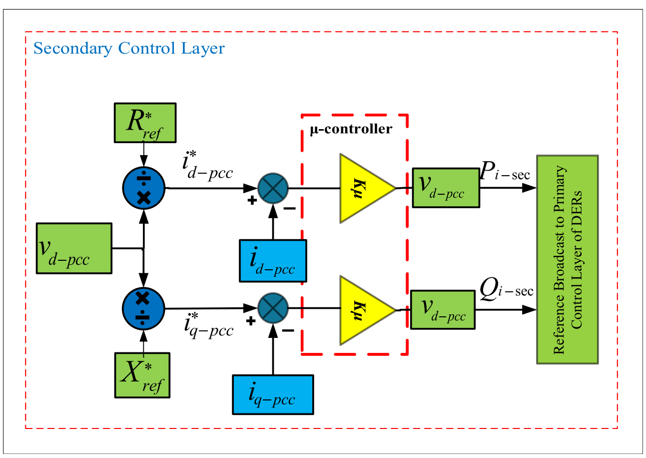


Fig. 3. Block diagram of the secondary control.

Here, (9a) and (9b) represent the apparent resistance and reactance at the PCC of ADN, respectively. Eq. (9a) and (9b) can be used by the TSO/DSO to calculate the apparent RX demand at PCC of ADN [23]. The apparent RX demand values can be used to produce $dq$-frame reference currents as given in (8). Using these reference values, the PCC of ADN can be controlled using an appropriate controller such that

$$\Delta i_{d-\text{pcc}} = (K_{p1})(i^*_{d-\text{pcc}} - i_{d-\text{pcc}}) \tag{10}$$

$$\Delta i_{q-\text{pcc}} = (K_{p2})(i^*_{q-\text{pcc}} - i_{q-\text{pcc}}). \tag{11}$$

Here, $K_{p1}$ and $K_{p2}$ are the required controllers to regulate the PCC of ADN. Furthermore, the output of the controller (Fig. 3) can be multiplied by the $d$-axis voltage at PCC to calculate the reference active and reactive power. The new expression is given as

$$P_{i\text{sec}-\text{ref}} = \Delta i_{d-\text{pcc}} * v_{d-\text{pcc}}; Q_{i\text{sec}-\text{ref}} = \Delta i_{q-\text{pcc}} * v_{d-\text{pcc}}. \tag{12}$$

Here, $P_{i\text{sec}-\text{ref}}$ and $Q_{i\text{sec}-\text{ref}}$ are the reference active and reactive powers dispatched to each DER.

## B. Proposed $\mu$-Synthesis

It is pertinent that, the controller given in (10) and (11) should be optimal and robust against the dynamics of the ADN. For this purpose, this subsection models the dynamics of the proposed system in order to design a concatenated plant model. The concatenated plant model can then be used to derive a robust controller that minimizes the $H_\infty$-norm of the closed-loop plant model even for uncertain conditions. To avoid redundancy, this study only considers the apparent R regulation, however, the same method can be used for apparent X regulation. Since, the secondary controller output is dispatched to the cluster of DERs, therefore, the generation from DERs can be considered as coupled to the secondary controller. Using the reference from secondary control layer, the dynamics of four DERs and a BESS (as per Fig. 1) in the proposed cluster can be expressed as [22]

$$\dot{P}_1 = -P_1/\tau_1 + P_{\text{sec}-\text{ref}}/\tau_1 \tag{13a}$$

$$\dot{P}_2 = -P_2/\tau_2 + P_{\text{sec}-\text{ref}}/\tau_2 \tag{13b}$$

$$\dot{P}_3 = -P_3/\tau_3 + P_{\text{sec}-\text{ref}}/\tau_3, \tag{13c}$$

$$\dot{P}_4 = -P_4/\tau_4 + P_{\text{sec}-\text{ref}}/\tau_4 \tag{13d}$$

$$\dot{P}_{\text{BESS}} = -P_{\text{BESS}}/\tau_5 + P_{\text{sec}-\text{ref}}/\tau_5. \tag{13e}$$

Here, $\tau$ denotes the moment of virtual inertia for each DER ($\tau_{1-5}$); $P_{\text{sec}-\text{ref}}$ is the active power dispatched from secondary control layer; and $P_1 - P_5$ is the active power from respective DERs. Following a disturbance, i.e., demand fluctuation at PCC/load variation within or outside ADN/active and reactive power variation from DERs, an error will emerge in (10) and (11). If the controller does not respond in a timely manner, the PCC will experience huge oscillations that may inflict negative consequences for the life of nearby equipment. In addition, the error induces new value for $P_{\text{sec}-\text{ref}}$ which is dispatched to each DER as a reference to follow. Hence, the active and reactive power regulation at each DER will be influenced by the oscillations faced by the PCC. The error at PCC can be expressed as

$$e_{\text{pcc}} = i_{d-\text{pcc}} - i^*_{d-\text{pcc}}. \tag{14}$$

From (6), the $d$-axis current at PCC can be expressed as

$$i_{d-\text{pcc}} = i_L - i_1 - i_2 - i_3 - i_4 - i_{\text{BESS}}. \tag{15}$$

The currents in terms of state variables (active power) from each DER can be written as

$$i_{d-\text{pcc}} = \frac{1}{1.5V_{d-\text{pcc}}}(P_L - P_1 - P_2 - P_3 - P_4 - P_{\text{BESS}}). \tag{16}$$

Here, $1/1.5V_{d-\text{pcc}}$ is considered as $\epsilon$ for the sake of simplicity. By inserting (16) in (14), the new expression for error can be written as

$$e_{\text{pcc}} = \epsilon * (P_L - P_1 - P_2 - P_3 - P_4 - P_{\text{BESS}}) - i^*_{d-\text{pcc}}. \tag{17}$$

Eq. (17) represents the error at apparent RX demand at PCC. The prime objective of this study is to regulate this error to zero with minimum overshoot and oscillations. For this purpose, the proposed state equations (13a)–(13e) and output equation (17) can be used to establish a concatenated plant model. Generally, the input and output equations of a system in a state-space model can be expressed as

$$\dot{x} = Ax + B_1 w + B_2 u; y = Cx + D_1 w + D_2 u. \quad (18)$$

Here, according to the proposed application, (13a)–(13e) is equivalent to the state input $\dot{x}$; and $e_{\text{pcc}}$ is equivalent to the output equation $y$; $u$ is equivalent to the control signal $P_{\text{sec-ref}}$ which is calculated by multiplying the output of controller with $v_{d-\text{pcc}}$; the exogenous inputs $(w)$ is given by $w = [w_1\ w_2\ w_3]$ which according to our model is $w = [\Delta i_{\text{error}}\ P_L\ i^*_{d-\text{pcc}}]$. Here, the error in the measured error signal is denoted by $\Delta i_{\text{error}}$ as shown in Fig. 25. The role of the aforementioned entities in the design loops can be observed in the plant model illustrated in Fig. 2. As a result of comparison between the proposed models and the generalized models, the obtained matrices can be written as

$$A = \begin{bmatrix} -1/\tau_1 & 0 & 0 & 0 & \\ 0 & -1/\tau_2 & 0 & 0 & \\ 0 & 0 & -1/\tau_3 & 0 & \\ 0 & 0 & 0 & -1/\tau_4 & \\ 0 & 0 & 0 & 0 & -1/\tau_5 \end{bmatrix}$$

$$B_1 = \begin{bmatrix} 0 & 0 \\ 0 & 0 \\ 0 & 0 \\ 0 & 0 \\ 0 & 0 \end{bmatrix}, B_2 = \begin{bmatrix} 1/\tau_1 \\ 1/\tau_2 \\ 1/\tau_3 \\ 1/\tau_4 \\ 1/\tau_5 \end{bmatrix}, D_2 = 0,$$

$$C = \begin{bmatrix} -\epsilon & -\epsilon & -\epsilon & -\epsilon & -\epsilon \end{bmatrix}, D_1 = \begin{bmatrix} \epsilon & -\epsilon \end{bmatrix}.$$

$B_1$ and $D_1$ has only two components because the exogenous input due to error in measured signal ($\Delta i_{\text{error}}$) is not involved at this point and will be considered eventually in the next step. Considering the concatenation of the input and output equations, a general matrix representation can be expressed as

$$P = \left[\begin{array}{c|cc} A & B_1 & B_2 \\ \hline C & D_1 & D_2 \end{array}\right].$$

To derive the $\mu$ synthesis-based controller, the linear fractional transformation (LFT) model is arranged as

$$\begin{bmatrix} \tilde{z} \\ \tilde{y} \end{bmatrix} = \tilde{P} \begin{bmatrix} \tilde{w} \\ u \end{bmatrix}. \quad (19)$$

Here, the main objective of the controller should be to minimize the impact of exogenous inputs $(\tilde{w})$ on the regulated outputs $(\tilde{z})$ of the concatenated plant model. In (19), the term $\tilde{P}$ is the concatenated plant model. Moreover, the corresponding input signal in terms of a controller and the output is given by $u = K_\mu * \tilde{y}$.

As per Fig. 2, the measured error signal is influenced by the exogenous input (inaccuracy of the sensing device) as

$$\tilde{y} = e_{\text{pcc}} + \zeta w_1 = \left[\begin{array}{c|cc} A & B_1 & B_2 \\ \hline C & D_1 & D_2 \end{array}\right] \begin{bmatrix} w \\ u \end{bmatrix} + \zeta w_1. \quad (20)$$

Here, the term $w_1$ is the exogenous input due to the inaccuracy in the measured error while the term $\rho$ is used to tune the intensity of the inaccuracy. With the newly added exogenous input, the output equation becomes

$$\tilde{y} = \left[\begin{array}{c|ccc} A & 0 & B_1 & B_2 \\ \hline C & \zeta & D_1 & D_2 \end{array}\right] \begin{bmatrix} w_1 \\ w \\ u \end{bmatrix}. \quad (21)$$

The regulated outputs shown in Fig. 2 of the proposed plant model can be written as

$$z_1 = W_F * \tilde{y}, \quad z_2 = \sigma u. \quad (22)$$

Here, $\sigma$ is the intensity controlling parameter of the input signal. A weighting function $(W_F)$ is used to penalize the dc values of the output error signal. The term $(W_F)$ gives extra flexibility in controlling the error signal. For the proposed model in Fig. 2, the generalized $(W_F)$ is given by

$$W_F = \left[\begin{array}{c|c} A_F & B_F \\ \hline C_F & D_F \end{array}\right]. \quad (23)$$

From (22), it can be observed that, the output of the weighting function is considered to be the new output of the error. Therefore, the regulated output after including the weighting function $(W_F)$ is rewritten as

$$z_1 = \left[\begin{array}{cc|ccc} A & 0 & 0 & B_1 & B_2 \\ B_F C & A_F & B_F\zeta & B_F D_1 & B_F D_2 \\ \hline D_F C & C_F & \zeta D_F & D_F D_1 & D_F D_2 \end{array}\right] \begin{bmatrix} w_1 \\ w \\ u \end{bmatrix}. \quad (24)$$

To derive the final concatenated plant model, (20)–(24) are combined as

$$\tilde{P} = \left[\begin{array}{cc|ccc} A & 0 & 0 & B_1 & B_2 \\ B_F C & A_F & B_F\zeta & B_F D_1 & B_F D_2 \\ \hline D_F C & C_F & \zeta D_F & D_F D_1 & D_F D_2 \\ 0 & 0 & 0 & 0 & \sigma \\ C & 0 & \zeta & D_1 & D_2 \end{array}\right], \quad (25)$$

At this point, $\tilde{P}$ holds all the entities of the system given in Fig. 2 except the controller. The proposed $\mu$ synthesis-based controller should be such that it minimizes the $H_\infty$-norm of the closed-loop LFT model. The $\mu$-synthesis problem is considered as suboptimal. Therefore, the norm of the closed-loop system, if minimized less than $\gamma = 2$, then the solution will be considered as suboptimal. The minimization of the $H_\infty$-norm of the LFT can be represented as $||\mathscr{F}(\tilde{P}, K)||_\infty < \gamma$.

### C. $\mu$-Synthesis Based Controller Derivation

The $\mu$ synthesis-based controller can be exploited to minimize the $H_\infty$-norm of the LFT model given as $||\mathscr{F}(\tilde{P}, K)||_\infty < \gamma$. For this purpose, MATLAB command "musyn" is used which yields a controller that minimizes the $H_\infty$-norm of the closed-loop transfer function (19). Provided the right dimensions of the concatenated plant model, and uncertainty percentage of the moment of inertia of DERs and BESS, the MATLAB command "musyn" yields a 16° transfer function of the newly derived controller.

The transfer function of a 16° controller makes it highly complex to be implemented physically. Controllers with higher degrees will require more sensors to perform in a physical world.

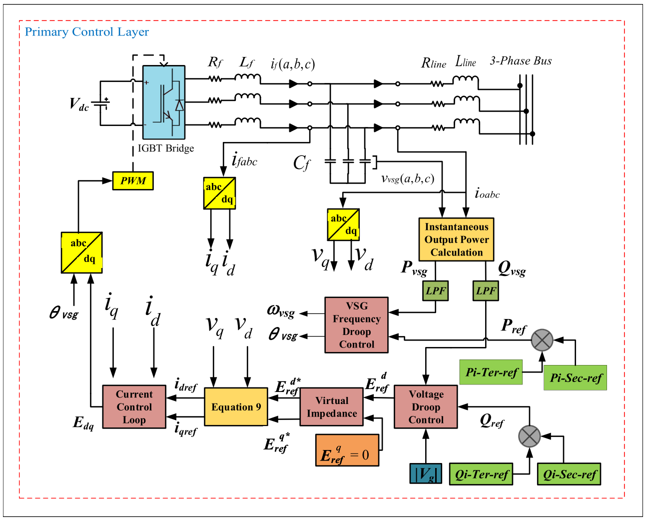


Fig. 4. Primary control layer.

Therefore, the controller is reduced using model order reduction. For this purpose, MATLAB command "minreal" is used to reduce the order of the controller. The reduced order is given as

$$K_{\mu} = \frac{210.53}{(s + 162.2)}. \tag{26}$$

The derived controller implementation in the proposed model is shown in the block diagram of the secondary controller, i.e., Fig. 3. The primary control layer receives active and reactive power references from the secondary and tertiary control layer as shown in Fig. 4. Each stage of the proposed hierarchical control strategy is described in Fig. 6. From Fig. 7, it can be observed that, the frequency response of the original controller (16° size) and the reduced controller is almost similar. This confirms that the reduced controller has similar attributes as the ones found in the original controller.

## D. Considering Uncertainty, Nominal Stability, and Performance

For the proposed concatenated plant model, $\pm 10\%$ uncertainty is considered for the values in $\tau_1 - \tau_5$. For a single VSG, $\pm 10\%$ uncertainty may not have a significant impact on the overall power system, however, for the whole coordinating cluster, $\pm 10\%$ uncertainty in moment of inertia of each VSG will have a prominent impact. The modeled uncertainty is inserted in the concatenated plant model as an upper linear fractional transformation. The uncertainty is represented by a $\Delta$ as shown in Fig. 5. To test the system under disturbances, the exogenous inputs ($\tilde{w}$) to the plant model are considered. The suboptimal controller solution should be such that the peak singular values of the closed-loop system are less than the pre-defined $\gamma$ which is typically kept at 2. This can be expressed as

$$||\mathscr{F}(\tilde{P}, K)||_{\infty} = \max_{\omega} \overline{\sigma}(\mathscr{F}(\tilde{P}, K)(j\omega)) < \gamma. \tag{27}$$

As shown in Fig. 8, the peak singular values of the closed-loop plant are less than two for all the frequencies and considering uncertainties, therefore, the performance of the controller is confirmed to be satisfactory. As a suboptimal solution is acquired through a controller that minimizes the $H_{\infty} -$ norm of the closed-loop system, this confirms that the system is internally stable under all the considered uncertainties using the derived $\mu$ controller.

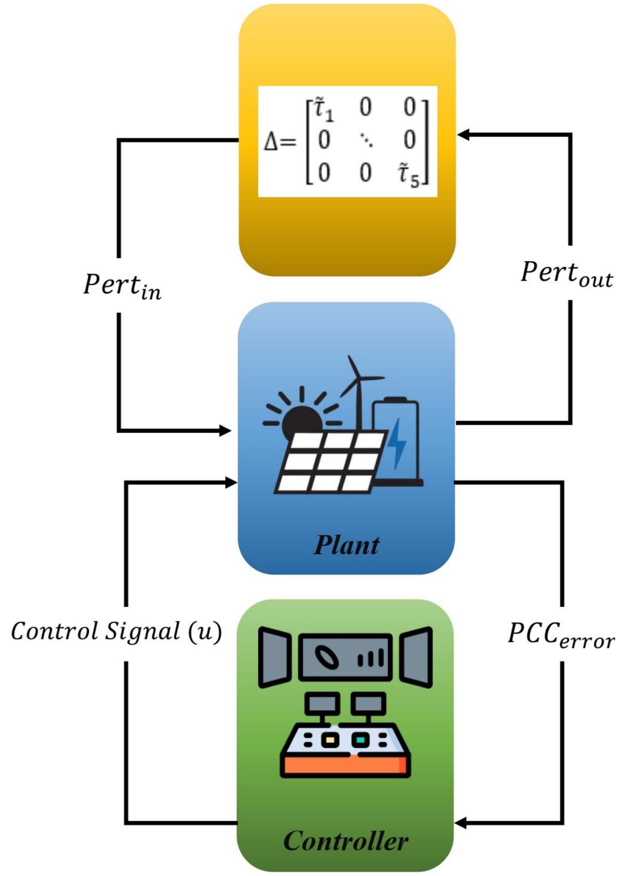


Fig. 5. Uncertainty modeling.

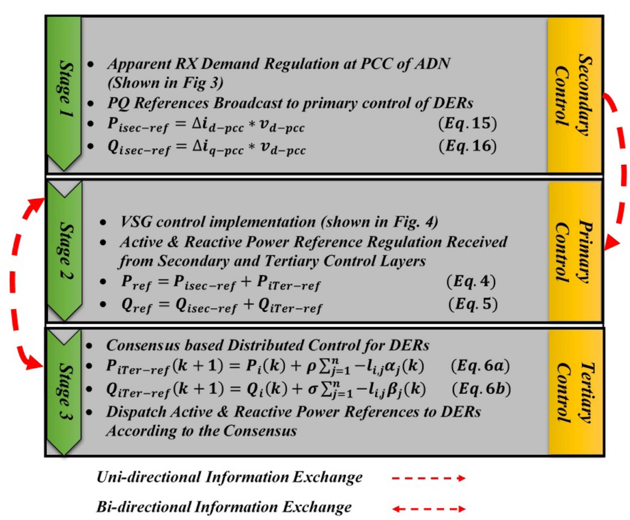


Fig. 6. Flowchart of the proposed strategy.

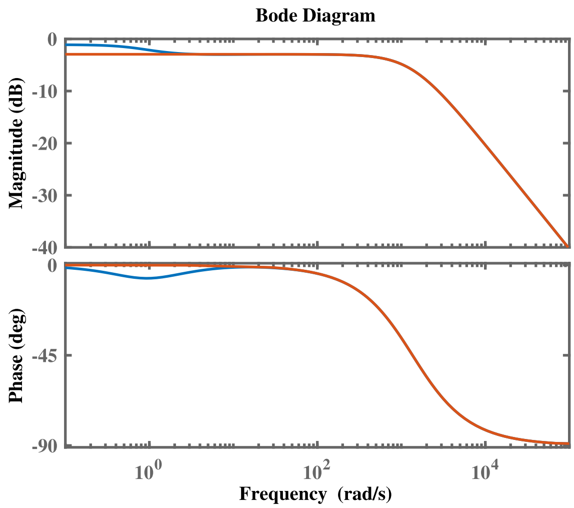


Fig. 7. Bode diagram of the original controller and the reduced controller.

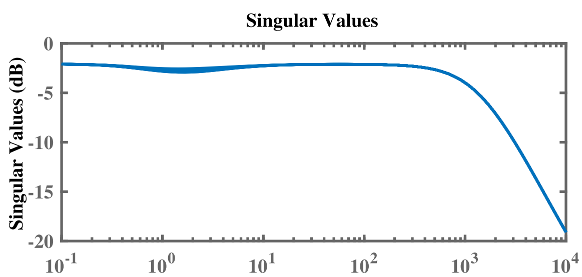


Fig. 8. Singular values of the closed-loop system across all the frequencies.

## IV. Numerical Simulation Results

The proposed test system given in Fig. 1 is validated in MATLAB/Simulink environment. The ADN in this figure is connected to a TLN so that the cluster of DERs is also aware of the dynamics of the TLN. The proposed ADN system is energized by four VSG controlled DERs and a BESS making the total capacity of the ADN to be 220 kVA. However, the BESS does not take part in active power sharing. In order to demonstrate a practical LV distribution network, the DERs are connected to high R/X ratio lines, i.e., above 2 [25]. The PQ coupling between VSGs is overcome using virtual impedance technique. Further detailed parameters of the proposed system are given in Table I. The power transformer of the substation is rated at 100 kW in order to demonstrate overwhelming power injection situation.

The simulation is tested for various case studies. For instance, in the beginning of the simulation (at $t = 0$ s), the active power coordination is intact while the reactive power coordination is not active. At this point, the power injection to the grid is according to the demand $R^*_{\text{ref}} = -7.254$ and $X^*_{\text{ref}} = -29.01$. Eq. (9a) and (9b) can be used to calculate the required RX references according to the active and reactive power needs. The reactive power coordination among DERs is activated at $t = 1.5$ s. For all the methods simulated in the upcoming sections, the active and reactive power convergence speed constant for all the DERs is kept at $\alpha = 1e5$ and $\beta = 1e5$, respectively. A constant power load of $P_{L2} = 40$ m and $Q_{L2} = 10$ kVAR is attached

TABLE I
System Parameters Utilized From [22]

| Parameters | VSG1 | VSG2 | VSG3 | VSG4 |
|---|---|---|---|---|
| Active power capacity (kW) | 50 | 40 | 55 | 65 |
| Reactive power capacity (kVAR) | 16 | 12.5 | 17.5 | 20.296 |
| Moment of inertia (J) | 3.03 | 1.622 | 3.5696 | 4.7466 |
| Damping coefficient (D) | 80 | 60 | 100 | 120 |
| Active power droop ($K_p$) | $985.96e^{-5}$ | $1232.45e^{-5}$ | $894.9e^{-5}$ | $758.4042e^{-5}$ |
| Reactive power droop ($K_q$) | $1.945e^{-3}$ | $2.4896e^{-3}$ | $1.778e^{-3}$ | $1.532e^{-3}$ |
| LPF time constant, $\tau$(s) | 0.01 | 0.01 | 0.01 | 0.01 |
| Reactive power inertia, ($K$) | 1/15 | 1/12 | 1/18 | 1/22 |
| Virtual resistance, ($R_v$) | 0.1Ω | 0.1Ω | 0.1Ω | 0.1Ω |
| Virtual inductance, ($L_v$) | 3 mH | 3 mH | 3 mH | 3 mH |
| Feeder R/X ratio, ($R_l/X_l$) | 3 | 6 | 4 | 5 |

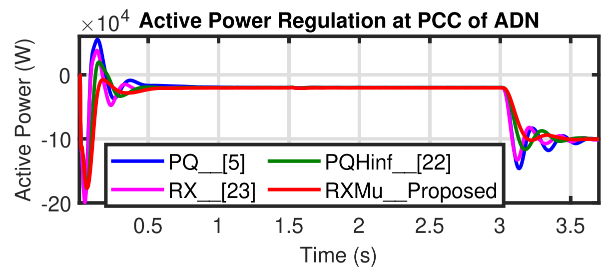


Fig. 9. Active power management at PCC of ADN.

to bus 6 while another plug and play load of $P_{L3} = 30$ kW and $Q_{L3} = 10$ kVAR is connected to the bus 3. For the sake of comparison, the state-of-the-art controllers are mentioned as: PQ regulation at PCC (from [5]) is denoted as PQ; RX regulation at PCC (from [23]) is denoted as RX; and $H_{\text{inf}}$ based controller (from [22]) regulation at PCC is denoted as PQHinf. The proposed controller is denoted as RXMu.

### A. Strengthening the Rigidness of PCC

If the management at PCC is carried in such a manner that the controller allows minimum magnitude of peak and least oscillations for the parameters under control, such as active power/reactive power/voltage, then the PCC is considered to be rigid. On the other hand, higher peaks and oscillations across the PCC shows lack of rigidness. Therefore, comparing between the state-of-the-art methods and the proposed method, the method that offers least oscillations and peak magnitude will be considered the most rigid technique.

Since, the active power, reactive power, and voltage at PCC can show how flexible or rigid the response at the PCC is, therefore, the results in terms of the aforementioned parameters are illustrated in Figs. 9 and 11. In Fig. 9, the active power injection at PCC is illustrated. At $t = 0$ s, the PCC demand is $R^*_{\text{ref}} = -7.254$ and $X^*_{\text{ref}} = -29.01$ which constitutes to an active power of approximately $-20$ kW and reactive power of $-5$ kVAR, respectively. From this figure it can be observed that, the transient during the initialization of the simulation is significantly larger for the PQ and RX method. The active power overshoot peak for PQ method is the worst performing followed

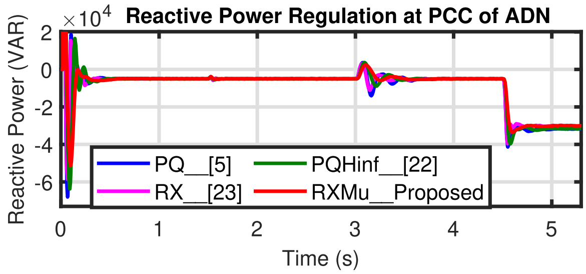


Fig. 10. Reactive power injection at PCC of ADN.

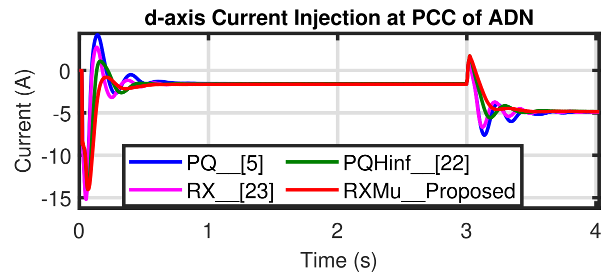


Fig. 12. $d$-axis current at PCC of ADN.

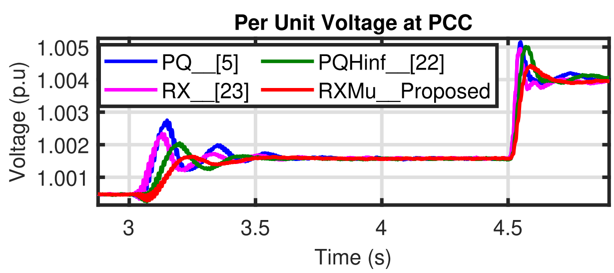


Fig. 11. Voltage assessment at PCC of ADN.

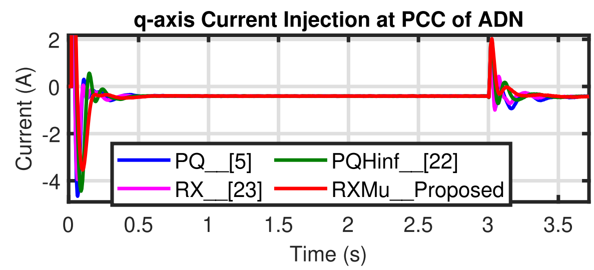


Fig. 13. $q$-axis current at PCC of ADN.

by RX method. On the other hand, the proposed controller, i.e., RXMu, significantly suppresses the overshoot compared and is almost performing similar to the PQHinf method. However, using the proposed method, the second peak observed in the same figure is far smaller in magnitude as compared to all the other methods. Furthermore at $t = 3$ s, the PCC demand is increased by reducing the reference apparent resistance value to $R^*_{\text{ref}} = -1.442$. At this point, the PCC active power injection is increased to $-100$ kW which is fulfilled by all the state-of-the-art techniques within one second. However, the PQ and RX methods allow several overshoots and undershoots before reaching the steady-state condition. The PQHinf method performs better than PQ and RX method in minimizing the overshoot and undershoots. However, the proposed RXMu method performs significantly superior by keeping the power overshoot minimum and requiring least amount of time to reach the steady-state condition compared to state-of-the-art methods.

Moreover, the reactive power injection at the beginning of the simulation can be observed in Fig. 10. In this figure, the state-of-the-art methods experience huge oscillations after $t = 0$ s which indicates the vulnerability of the voltage deviation for larger disturbances. On the contrary, using the proposed technique it can be observed that the reactive power response allows minimum oscillations and settles down at the steady-state condition shortly after the undershoot. Here, the superiority between the proposed technique and the state-of-the-art techniques is obvious. At $t = 4.5$ s, the reactive power demand is increased by reducing the value of reference apparent reactance to $X^*_{\text{ref}} = -4.835$. At this point, the proposed technique again outclass the old techniques by transitioning to a new reactive power injection value with minimum overshoot. The influence of the reactive power can be vividly understood by observing the response of the voltage at PCC as shown in Fig. 11. In this figure, the oscillations and peak overshoots/undershoots at transients clearly indicate the lack of rigidness of the PCC under state-of-the-art techniques. On the contrary, the proposed method clearly outperforms the previously proposed methods by not only minimizing the oscillations but also reducing the peak overshoots/undershoots as well. The above analysis shows that, the proposed method greatly enhances the damping of oscillations at PCC of ADN thus improving the rigidness of the PCC. It is recalled that, reducing the oscillations and overshoots at PCC can greatly reduce the stress on the substation transformer and enhance the life expectancy of expensive equipment.

### B. *Influence of Uncertain Load Variation*

In theory, the PCC of ADN should be rigid enough to handle huge load variations. For this purpose, this subsection tests the proposed strategy under the 60% (for a 100 kW substation transformer) load variation and 40 kW of PCC reference variation based case study. In this manner, the influence of load variation along with variation of power at PCC can be tested on the PCC of ADN. For this case study, the PCC currents are simulated in Figs. 12 and 13. These figures already illustrate a better transient response for the proposed strategy during the start of simulation. Whereas, the rest of the methods experience comparatively higher oscillations which is an indication of poor performance as compared to the proposed method. However, the proposed method allows the first undershoot peak similar to PQHinf method while the PQ and RX methods perform worse than the proposed method and PQHinf method. Nevertheless, the proposed RXMu method still smoothly converge to the steady-state condition while the rest of the methods allow a significant overshoot before converging to the steady-state condition. Similar to the reactive power response in the previous section, the response of current under the state-of-the-art methods also experience significant oscillations as compared to the proposed

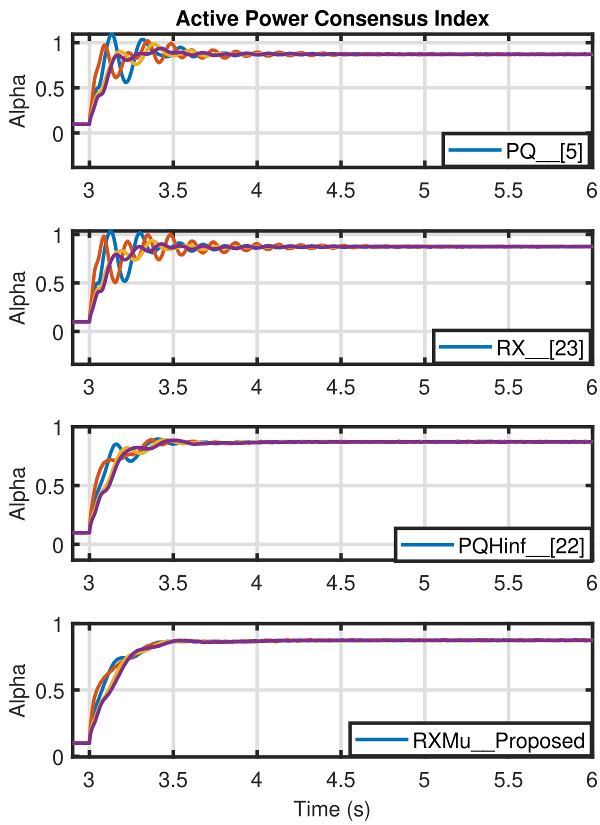


Fig. 14. Active power consensus index: (a) RXmode proportional controller; (b) RXmode PI controller; (c) PQmode; (d) RXmode with Proposed Mu-Synthesis Controller.

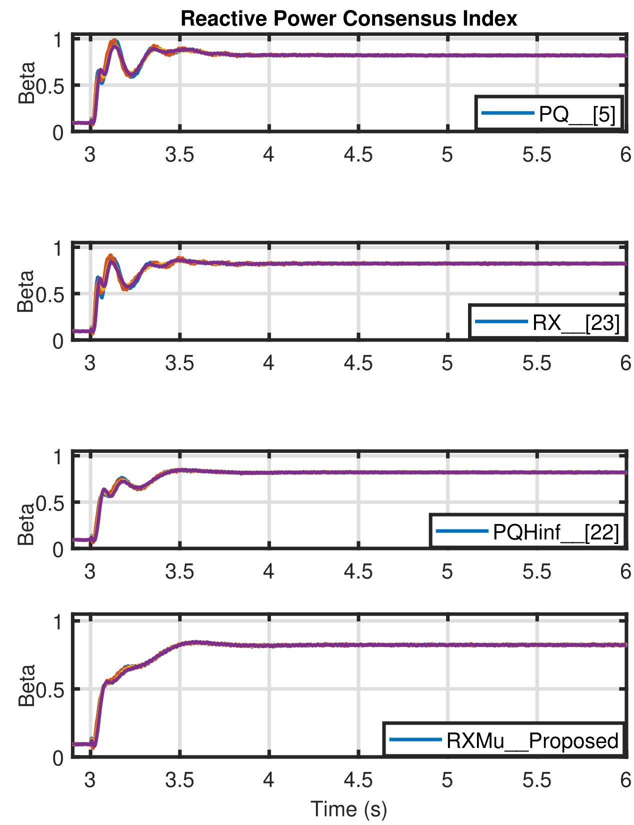


Fig. 15. Reactive power consensus index: (a) RXmode proportional controller; (b) RXmode PI controller; (c) PQmode; (d) RXmode with Proposed Mu-Synthesis Controller.

technique which smoothly converges to the steady-state condition after the second peak. In Fig. 13, it can be observed that, not only the undershoot response is improved using the proposed method, but also the reactive power converges to the steady-state without further overshoots. On the contrary, the state-of-the-art methods experience significant overshoots before converging to the steady-state. Here, even minor deviations should not be underestimated as these values are according to the kW magnitude.

Since, the load variation changes the active and reactive power generation from DERs as well, therefore, the coordination control among DERs need to be observed as well. Since, this study used consensus based distributed control strategy, therefore, the consensus index for active and reactive power under all the demonstrated strategies is presented in Figs. 14 and 15. In Fig. 14(a)–14(b), it can be observed that at $t = 3$ s, the PQ and RX methods allow significant oscillations before settling down to a new consensus index value. While the PQHinf method comparatively minimizes the oscillations up to some extent. On the contrary, the consensus index of the proposed method in Fig. 14(d) allows a comparatively smoother transition towards a new consensus index. From this figure it can be observed that the proposed method offers significant improvement over the PQ and RX methods while slight improvement over the PQHinf method. The smooth transition towards a new consensus index is an important trait as the power-electronics converters have limited capacities. Huge oscillations during transients can overwhelm the power-electronics switches and thus reducing the life expectancy of the power electronics converters. Similarly, the response of consensus index for the reactive power demand variation is demonstrated in Fig. 15(a)–(d). A huge overshoot/undershoot can be observed at $t = 3$ s of Fig. 15(a)–15(b) while comparatively lower oscillations for Fig. 15(c). On the other hand in Fig. 15(d), the proposed strategy allows a smooth convergence towards a new consensus index with minimum overshoots.

### C. Response of the Farthest DER and Frequency Deviation

It is well established that, the DERs located far away from the substation transformer will have more voltage to reactive power sensitivity as compared to the DER located near the substation transformer. Therefore, this subsection will compare the active and reactive power response of farthest located DER in order to demonstrate sensitive testing conditions for the proposed strategy. In the proposed test system, the DER2 is erected at longest distance from the substation transformer. The active and reactive power of DER2 are illustrated in Figs. 16 and 17. From these figures it can be observed that, the PQ and RX techniques allow huge oscillations in active and reactive power of DERs during transient right after $t = 0$ s. This can be severely expensive for the power electronics converters due

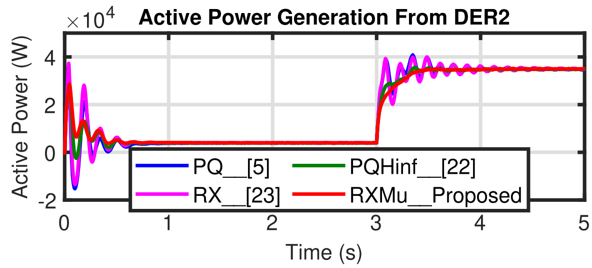


Fig. 16. Active power response assessment of DER2.

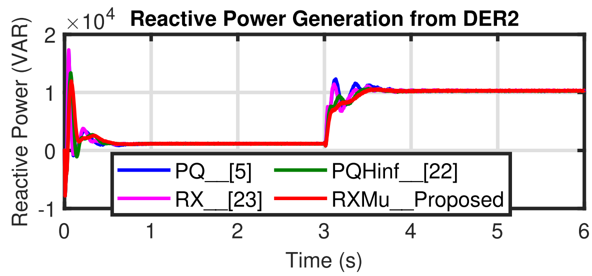


Fig. 17. Reactive power response assessment of DER2.

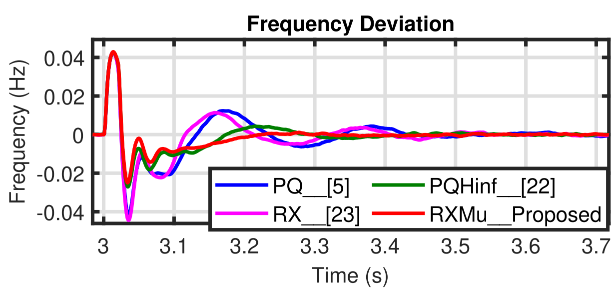


Fig. 18. Effect of demand fluctuations at PCC on the frequency deviation.

to their limited current carrying capacity. If the converter is already operated close to maximum rating then these oscillations can overwhelm the switches during transients. For instance, at $t = 3$ s in Fig. 16, the active power increase in PCC demand has caused severe oscillations when PQ and RX methods are applied. However, using the PQHinf method, the oscillations are damped compared to the PQ and RX method. Nevertheless, using the proposed RXMu method, these oscillation are significantly suppressed and the new steady-state generation point is achieved with a smoother transition as compared to the other demonstrated methods. Similar behavior can be observed for reactive power generation variation in Fig. 17 as well. Here, as expected, the proposed RXMu strategy outperforms the other methods in terms of suppressing the overshoots and undershoots in power transition.

It is understandable that, with fluctuations in power, the frequency of the system will also be influenced. Therefore, this subsection also illustrates the results of the frequency deviation and RoCoF in Figs. 18 and 19. At $t = 0$ s in Fig. 18, the frequency oscillations for the PQ and RX method are an indication of lack of rigidness at PCC. The power oscillations makes the frequency nervous during disturbances. The PQHinf method experience comparatively lower amplitude of peak in frequency deviation

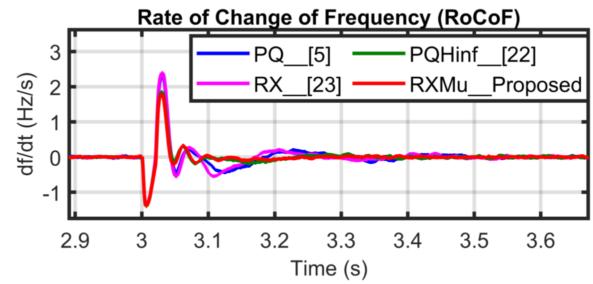


Fig. 19. Rate of change of frequency (RoCoF).

as compared to the PQ and RX method. On the contrary, the proposed RXMu technique successfully minimizes the peak oscillations. Although, the PQHinf has a minor frequency amplitude difference with the proposed RXMu technique, nevertheless, the proposed method outperforms PQHinf method by in terms of smooth transition to steady-state condition. In addition, the RoCoF in Fig. 19 also demonstrates a significant improvement for the proposed method as compared to the state-of-the-art methods. It is pertinent to mention that, the grid codes for RoCoF limit for several countries are generally kept at 2 for a 500 ms time window [26]. Beyond 2, the RoCoF relays trigger the circuit breaker to disconnect the DER. Therefore, the proposed method greatly overcomes this undesired situation by using only the control strategy and without upgrading expensive infrastructure.

## V. Conclusion

This study proposes a $\mu$ synthesis-based robust controller to enhance the rigidness of the apparent RX demand regulation at PCC of ADN. First, an extension of the mathematical model is presented in terms of error in RX demand regulation at PCC of ADN. Then, the extended mathematical model is utilized to develop a concatenated plant model including the uncertainties in the moment of inertia parameters. To minimize the $H_\infty$-norm of the closed-loop system, a $\mu$ synthesis-based robust controller is derived. Moreover, it was validated through stability analysis and performance analysis that using the proposed controller, the closed-loop system remains stable under uncertainties in moment of inertia of the whole cluster of DERs. Furthermore, it was demonstrated through extensive simulations that, the proposed method outperforms the state-of-the-art methods in terms of suppressing the overshoots and undershoots at the PCC of ADN. In this manner, it was confirmed that minimizing the closed-loop gain of the proposed system can enhance the rigidness of the PCC. Quantitatively, the PQ and apparent RX method allows RoCoF beyond 2 Hz/s while the proposed method and the PQHinf method restricts the RoCoF below the 2 Hz/s threshold. However, the proposed offer superior frequency deviation and RoCoF settling time compared to the state-of-the-art methods which is an important trait for modern grid codes due to increasing penetration levels of IRESs.

In terms of future work, this study suggests that the time delay aspect of communication signals should be considered as an uncertainty for deriving the closed-loop controller. The time-delay aspect should be involved in derivation of the mathematical model of the ADN.

## REFERENCES


[1] J. B et al., "Renewables 2023 global status report," REN21, 2023. [Online]. Available: https://www.ren21.net/gsr-2023/

[2] A. Sangwongwanich, Y. Yang, F. Blaabjerg, and D. Sera, "Delta power control strategy for multistring grid-connected PV inverters," *IEEE Trans. Ind. Appl.*, vol. 53, no. 4, pp. 3862–3870, Jul./Aug. 2017.

[3] S. Fahad, A. Goudarzi, and J. Xiang, "From grid feeding to grid supporting converters: A constant power active distribution network perspective," in *Proc. IEEE 29th Int. Symp. Ind. Electron.*, 2020, pp. 862–867.

[4] A. Fathi, Q. Shafiee, and H. Bevrani, "Robust frequency control of microgrids using an extended virtual synchronous generator," *IEEE Trans. Power Syst.*, vol. 33, no. 6, pp. 6289–6297, Nov. 2018.

[5] S. Fahad, A. Goudarzi, and J. Xiang, "Demand management of active distribution network using coordination of virtual synchronous generators," *IEEE Trans. Sustain. Energy*, vol. 12, no. 1, pp. 250–261, Jan. 2021.

[6] N. T. Mbungu, A. A. Ismail, M. AlShabi, R. C. Bansal, A. Elnady, and A. K. Hamid, "Control and estimation techniques applied to smart microgrids: A review," *Renewable Sustain. Energy Rev.*, vol. 179, 2023, Art. no. 113251. [Online]. Available: https://www.sciencedirect.com/science/article/pii/S1364032123001077

[7] F. Bandeiras, E. Pinheiro, M. Gomes, P. Coelho, and J. Fernandes, "Review of the cooperation and operation of microgrid clusters," *Renewable Sustain. Energy Rev.*, vol. 133, Nov. 2020, Art. no. 110311.

[8] L. Meng, E. R. Sanseverino, A. Luna, T. Dragicevic, J. C. Vasquez, and J. M. Guerrero, "Microgrid supervisory controllers and energy management systems: A literature review," *Renewable Sustain. Energy Rev.*, vol. 60, pp. 1263–1273, Jul. 2016.

[9] K. T. Tan, P. L. So, Y. C. Chu, and M. Z. Q. Chen, "Coordinated control and energy management of distributed generation inverters in a microgrid," *IEEE Trans. Power Del.*, vol. 28, no. 2, pp. 704–713, Apr. 2013.

[10] Y. Mishra, S. Mishra, and F. Li, "Coordinated tuning of DFIG-based wind turbines and batteries using bacteria foraging technique for maintaining constant grid power output," *IEEE Syst. J.*, vol. 6, no. 1, pp. 16–26, Mar. 2012.

[11] H. Beltran, E. Bilbao, E. Belenguer, I. Etxeberria-Otadui, and P. Rodriguez, "Evaluation of storage energy requirements for constant production in PV power plants," *IEEE Trans. Ind. Electron.*, vol. 60, no. 3, pp. 1225–1234, Mar. 2013.

[12] N. Jabalameli, M. A. Masoum, F. Shahnia, and T. H. Mehr, "Impact of battery rating on performance of rooftop PV supporting household loads, regulating PCC voltage and providing constant output power to grid," in *Proc. Australas. Universities Power Eng. Conf.*, 2013, pp. 1–6.

[13] H. Xin, M. Zhang, J. Seuss, Z. Wang, and D. Gan, "A real-time power allocation algorithm and its communication optimization for geographically dispersed energy storage systems," *IEEE Trans. Power Syst.*, vol. 28, no. 4, pp. 4732–4741, Nov. 2013.

[14] N. R. Tummuru, M. K. Mishra, and S. Srinivas, "Dynamic energy management of renewable grid integrated hybrid energy storage system," *IEEE Trans. Ind. Electron.*, vol. 62, no. 12, pp. 7728–7737, Dec. 2015.

[15] T. Zhao and Z. Ding, "Distributed finite-time optimal resource management for microgrids based on multi-agent framework," *IEEE Trans. Ind. Electron.*, vol. 65, no. 8, pp. 6571–6580, Aug. 2018.

[16] H. Pourbabak, J. Luo, T. Chen, and W. Su, "A novel consensus-based distributed algorithm for economic dispatch based on local estimation of power mismatch," *IEEE Trans. Smart Grid*, vol. 9, no. 6, pp. 5930–5942, Nov. 2018.

[17] X. Yan, A. Rasool, F. Abbas, H. Rasool, and H. Guo, "Analysis and optimization of the coordinated multi-VSG sources," *Electronics*, vol. 8, no. 1, 2018, Art. no. 28. [Online]. Available: https://www.mdpi.com/2079-9292/8/1/28

[18] P. Hu et al., "Coordinated control of multiple virtual synchronous generators in mitigating power oscillation," *Energies*, vol. 11, no. 10, 2018, Art. no. 2788. [Online]. Available: https://www.mdpi.com/1996-1073/11/10/2788

[19] Y. Hirase et al., "Decentralised and interlink-less power interchange among residences in microgrids using virtual synchronous generator control," *Appl. Energy*, vol. 228, pp. 2437–2447, 2018. [Online]. Available: http://www.sciencedirect.com/science/article/pii/S0306261918311401

[20] G. Yao, Z. Lu, Y. Wang, M. Benbouzid, and L. Moreau, "A virtual synchronous generator based hierarchical control scheme of distributed generation systems," *Energies*, vol. 10, 2017, Art. no. 2049.

[21] Z. Yang, Y. Li, and J. Xiang, "Coordination control strategy for power management of active distribution networks," *IEEE Trans. Smart Grid*, vol. 10, no. 5, pp. 5524–5535, Sep. 2019.

[22] S. Fahad, A. Goudarzi, P. Siano, and J. Xiang, "A novel method for improving the power response of a single-controllable VSG-based active distribution network," *CSEE J. Power Energy Syst.*, doi: 10.17775/CSEE-JPES.2022.07380.

[23] S. Fahad, A. Goudarzi, Y. Li, and J. Xiang, "A coordination control strategy for power quality enhancement of an active distribution network," *Energy Rep.*, vol. 8, pp. 5455–5471, 2022. [Online]. Available: https://www.sciencedirect.com/science/article/pii/S2352484722007776

[24] H. Wang, X. Ding, X. Wan, and Z. Guo, "Optimal-consensus-based event-triggered control strategy for island AC microgrids," *IEEE Syst. J.*, vol. 17, no. 3, pp. 3682–3693, Sep. 2023, doi: 10.1109/JSYST.2022.3220962.

[25] J. D. Kooning, J. V. de Vyver, J. D. D. Kooning, T. L. Vandoorn, and L. Vandevelde, "Grid voltage control with distributed generation using online grid impedance estimation," *Sustain. Energy, Grids Netw.*, vol. 5, pp. 70–77, Mar. 2016.

[26] PPA Energy and TNEI, "Rate of change of frequency (ROCOF): Review of TSO and generator submissions," Final Rep., May 2013. [Online]. Available: https://www.cru.ie/wp-content/uploads/2013/07/cer13143-appa-tnei-rocof-final-report.pdf